Available online at www.sciencedirect.com
ScienceDirect
Remote Sensing of Environment 106 (2007) 75–88
Remote Sensing of Environment
www.elsevier.com/locate/rse

Development of a winter snow water equivalent algorithm using in situ passive microwave radiometry over snow-covered first-year sea ice

A. Langlois *, D.G. Barber, B.J. Hwang

Centre for Earth Observation Science (CEOS), Clayton H. Riddell Faculty of Earth, Environment and Resources, Department of Environment and Geography, Wallace Building, University of Manitoba, Winnipeg, Manitoba, Canada R3T 2N2

Received 29 March 2006; received in revised form 26 July 2006; accepted 27 July 2006

Abstract

A snow water equivalent (SWE) algorithm has been developed for thin and thick snow using both in situ microwave measurements and snow thermophysical properties, collected over landfast snow covered first-year sea ice during the Canadian Arctic Shelf Exchange Study (CASES) overwintering mission from December 2003 to May 2004. Results showed that the behavior of brightness temperatures (T_bs) in thin snow covers was very different from those in a thick snowpack. Microwave SWE retrievals using the combination of T_b 19 GHz and air temperature (multiple regression) over thick snow are quite accurate, and showed very good agreement with the physical data ($R^2=0.94$) especially during the cooling period (i.e., from freeze up to the minimum air temperature recorded) where the snow is dry and cold. Thin snow SWE predictions also showed fairly good agreement with field data ($R^2=0.70$) during the cold season. The differences between retrieved and in situ SWE for both thin and thick snow cover are mainly attributable to the variations in air temperature, snow wetness and spatial heterogeneity in snow thickness.

Keywords: Snow water equivalent; Passive microwave; First-year sea ice; Snow thickness; Surface-based radiometer; Arctic

1. Introduction

The Arctic is thought to be an area where we can expect to see the first and strongest signs of global-scale climate variability and change (IPCC, 2001). This is due to a variety of strong feedbacks (e.g., the sea ice-albedo feedback, sea ice-cloud-albedo feedback, etc.), which occur in this region (Francis et al., 2005; Rothrock & Zhang, 2005). Central to these feedbacks is the ocean–sea ice–atmosphere (OSA) interface. The OSA plays a critical role in surface energy, mass and gas exchange and thus plays a central role in how the marine cryosphere responds to climate change.

Snow is arguably the most important element of the OSA interface as it controls both radiative and conductive exchanges across this interface (e.g., Powell et al., 2005). In particular, snow regulates heat transfer between the atmosphere and ocean due to its low thermal conductivity (Arons & Colbeck, 1995; Sturm et al., 2002), playing a dominant role in the surface energy balance (Eiken, 2003; Moritz & Perovich, 1996; Sturm et al., 2002). Physical properties of snow such as snow water equivalent (SWE), temperature and brine volume control the amount of solar energy absorbed within the snow and sea ice (e.g., Barber & Thomas, 1998; Warren et al., 1999; Zhou & Li, 2002). Consequently, changes in snow thermophysical properties during winter can substantially alter the surface radiative properties and the energy balance (e.g., Barber et al., 1998; Mundy et al., 2005; Welch & Bergmann, 1989) as well as the timing of annual freezing/melting of sea ice (Boer et al., 2000; Flato & Brown, 1996; Ledley, 1991).

Microwave remote sensing has proved to be a useful tool to estimate SWE remotely from space as it is independent from cloud cover and light conditions (e.g., Golden et al., 1998; Ulaby et al., 1986), and the high sensitivity of microwave emission to the changes in dielectric properties in snow (i.e., the changes in thermophysical properties). Many studies have examined the relationship between SWE and T_b over land (e.g., Chang et al., 1982; Comiso et al., 1989; Derksen et al., 2005; Kunzi et al., 1982; Pulliainen & Hallikainen, 2001; Tait, 1998;

* Corresponding author. Tel.: +1 204 474 6961; fax: +1 204 474 7699.
E-mail address: umlangl2@cc.umanitoba.ca (A. Langlois).

0034-4257/$ - see front matter © 2006 Elsevier Inc. All rights reserved.
doi:10.1016/j.rse.2006.07.018

Walker & Goodison, 1993, Walker & Silis, 2002), and very limited work has been done over first-year sea ice (Markus & Cavalieri, 1998). Amongst the difficulties, we denote vertical, diurnal and seasonal changes in snow physical properties (e.g., Barber et al., 1995; Langlois et al., in press), since changes in snow microstructure due to metamorphic processes change the microwave emission especially at higher frequencies such as 37 and 85 GHz (e.g., Armstrong et al., 1993; Grenfell & Lohanick, 1985; Lohanick, 1993). The precision of the SWE estimation is also affected by the changes in the liquid water content in snow, which readily modifies the snow emissivity (Drobot & Barber, 1998).

Extensive work estimating snow thickness using passive microwave radiometry from satellite remote sensing has been conducted since the 1980s (e.g., Cavalieri & Comiso, 2000). In situ studies on snow depth distribution over sea ice (e.g., Comiso et al., 1989; Markus & Cavalieri, 1998) showed fairly good agreement between estimated and measured data. Some studies looked specifically at SWE over first-year sea ice using data from ground-based passive microwave radiometers (Barber et al., 2003; Drobot & Barber, 1998) and results showed that 37 GHz is the most appropriate frequency to estimate SWE in snow depth averaging 20 cm.

In this study, we examine the physical, electrical and microwave properties of snow over landfast first-year sea ice in a study focused on development of a sea ice snow water equivalent (SWE) retrieval algorithm. We separate a naturally occurring winter snowpack into thin (~0–15 cm) and thick (~30–60 cm) due to their significantly different thermophysical characteristics (Langlois et al., in press) and corresponding

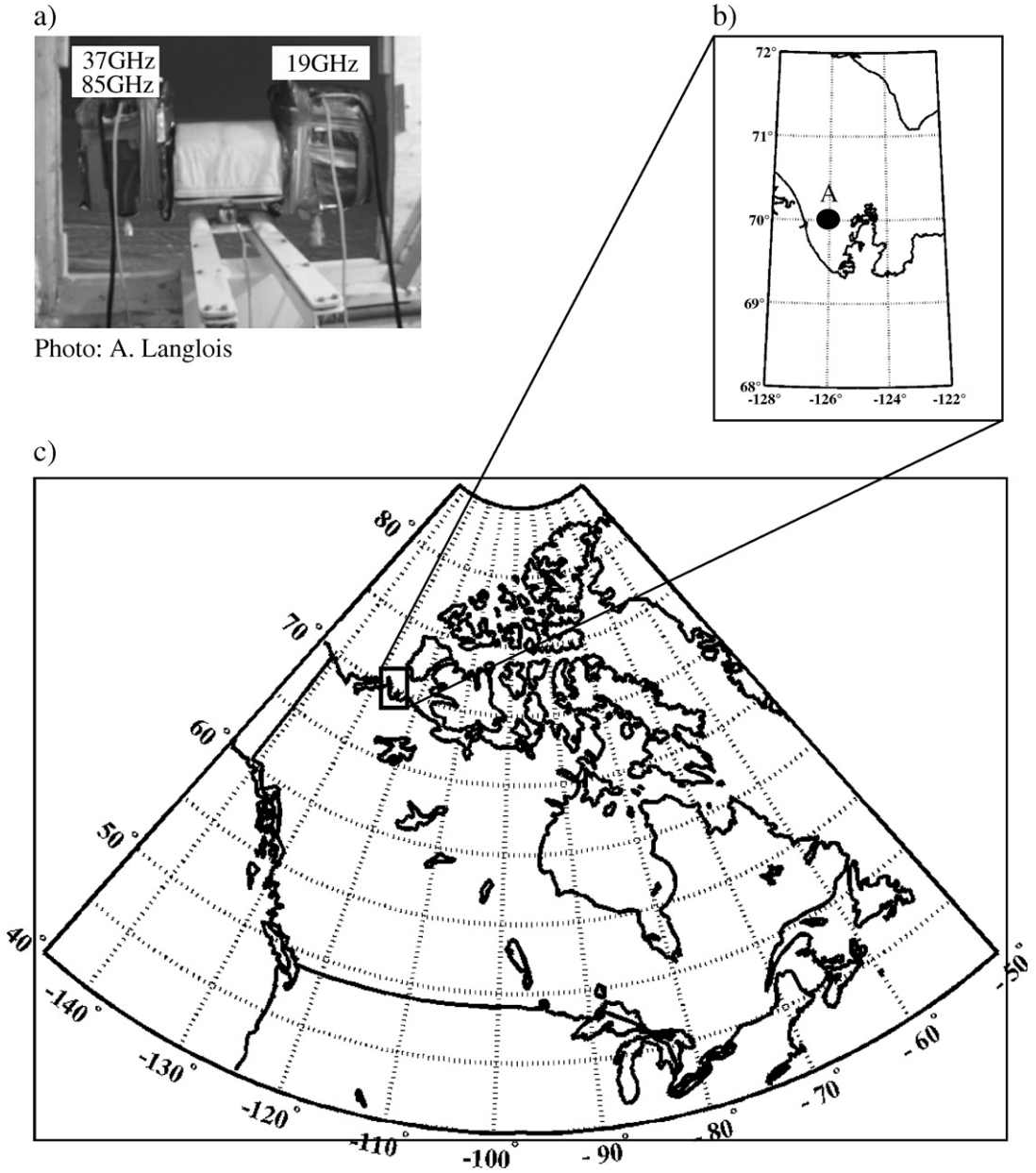

Fig. 1. Physical setup of the surface-based radiometers (SBR) mounted on the port side of the CCGS Amundsen (a) and study location in Franklin Bay, NWT (b and c).

difference in microwave T_bs (Rosenfeld & Grody, 2000). To constrain our analysis we focus on two interconnected objectives: (a) to describe how snow thermophysical properties affect passive microwave emission and (b) to develop new statistical SWE algorithms for both thin and thick snowpacks over first-year sea ice using winter in situ passive microwave emission for snow on landfast sea ice.

2. Data and methods

We collected data for this study as part of the Canadian Arctic Shelf Exchange Study (CASES) overwintering site between December 6, 2003, and May 7, 2004. Detailed in situ measurements were made of snow thermodynamically driven physical properties (thermophysical properties) such as thickness, density, salinity, grain size/shape, temperature, water in liquid phase and brine volume. Details of the temporal and spatial evolution of the thermophysical properties have been published elsewhere (Langlois et al., in press). In situ microwave properties (microwave emissivity and brightness temperature (T_bs)) were collected diurnally (morning–noon–afternoon) every second day. A surface-based radiometer (SBR) was installed about 12 m above the surface onboard the Canadian Coast Guard research icebreaker Amundsen, (Fig. 1a). The ship was frozen about 20 km offshore into a landfast pan of smooth first-year sea ice in Franklin Bay, Northwest Territories, Canada (Fig. 1b and c).

The snow physical data and the brightness temperatures were partitioned into two 'seasonal periods' (cooling and warming period) separated by the coldest day on day 58 (Fig. 2). A detailed description of the study site and sampling strategy can be found in Langlois et al. (in press).

2.1. Snow data

Snow physical data were sampled within an undisturbed area in close proximity to the SBR field of view on the port side of the ship (Fig. 1a). A total of 158 snowpits were completed throughout the sampling period (90 thin and 68 thick). Snow pits were excavated diurnally every second day at areas of thin (4–10 cm) and thick (10–80 cm) snow covers between December 6, 2003, and May 7, 2004. We arranged the sampling so that thin and thick snowpacks would be sampled throughout the study period. These thickness categories were selected to investigate the relationship between the evolution of snow overburden and the rates of grain metamorphism, and thermally dependent physical properties evolution of the snowpack. The snowpits were separated in layers where the 'vertical' changes were significant for at least two snow thermophysical properties. Consequently, thin snow covers were composed of three layers throughout the sampling season as thick snow covers evolved from 4 to 8 layers as the thickness increased significantly (Langlois et al., in press).

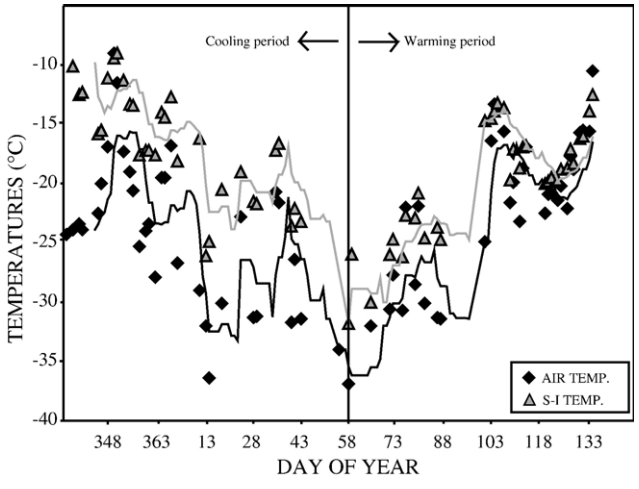

Fig. 2. Air and snow/sea ice (S-I) interface temperatures temporal evolution for thin snow covers (the lines represent a 2-day moving average on the temperatures).

The complex permittivity (or interchangeably known as the complex dielectric constant) of snow (ε^*) can be expressed as:

$$\varepsilon^* = \varepsilon' - j\varepsilon'', \tag{1}$$

where ε' represents the permittivity, ε'' the dielectric loss, and $j=\sqrt{-1}$ (Ulaby et al., 1986). Permittivity represents the ability of a material to permit incident energy through its volume, whereas dielectric loss represents the material's ability to dissipate that same energy. Models of snow dielectric properties usually consider two phases: (a) dry snow (low dielectric constant), which is a mixture of ice and air and contains no liquid water, and (b) wet snow (high dielectric constant), which is a mixture of ice, air and liquid water.

Both permittivity and dielectric loss of snow over first-year sea ice was calculated from a dielectric mixture model (Barber et al., 1995) of the form proposed by Polder-Van Santen and later modified by de Loor (Drinkwater & Crocker, 1988; Matzler, 1987; Ulaby et al., 1986). Fractional volumetric liquid water content (snow wetness (%)), which affects the dielectric properties, was calculated using a capacitance plate that measures increased conductivity of the volume due to the presence of liquid water.

Wetness values (W_v) below 1% were considered 'dry' and the model then treated brine as the "inclusion dielectric" within a dry snow "host dielectric" (Barber et al., 1995, after Matzler, 1987, and Drinkwater & Crocker, 1988). The complex dielectric constant of the mixture (Eq. (2)) can be calculated using the dielectric constant of both dry snow and brine. The dielectric constant of dry snow ($\varepsilon_{ds}*$) was calculated using the empirical model from Hallikainen and Winebrenner (1992). The permittivity and dielectric loss of the brine ε'_b and ε''_b are used to calculate ε_b^*, the complex dielectric constant of brine found and modeled using a Debye form of the model.

$$\Delta\varepsilon^*_{dry} = \chi \cdot V_b \left\{ \frac{\varepsilon^*_b - \varepsilon^*_{ds}}{1 + \left[\frac{\varepsilon^*_b - 1}{\varepsilon^*_{ds}}\right] \cdot A_0} \right\} \tag{2}$$

Snow wetness over 1% was considered 'wet' snow, where the permittivity (ε'_{wet}) and dielectric loss (ε''_{wet}) are independent of volume temperature and salinity. The wet mixture is

composed of dry snow ("host dielectric") and liquid water ("inclusion dielectric"). The permittivity ε'_{ws} (Eq. (3)) and dielectric loss ε''_{ws} (Eq. (4)) of wet snow was then calculated using the permittivity and dielectric loss of both dry snow and pure water (Tiuri et al., 1984) where:

$$\varepsilon'_{ws} = \varepsilon'_{ds} + \varepsilon'_{w} \cdot (0.1W_v + 0.8W_v^2) \quad (3)$$

$$\varepsilon''_{ws} = \varepsilon''_{w} \cdot (0.1W_v + 0.8W_v^2) \quad (4)$$

Both wet and dry snow dielectric constant calculations are dependent upon snow density and the frequency used.

2.2. Passive microwave

2.2.1. Surface-based radiometer measurements

The surface-based radiometer (SBR) receives vertically and horizontally polarized microwave emission at 19, 37 and 85 GHz with 15° beamwidth antennas (Asmus & Grant, 1999). Brightness temperatures for all three frequencies at both vertical and horizontal polarization were measured at a fixed incidence angle of 53° (approximately the same incidence angle used for spaceborne sensors: SMMR, SSM/I and AMSR-E), and also from multi-angular measurements between the incidence angle of 30° and 70° with a 5° increment. Absolute calibration for the measured brightness temperatures was done following Grenfell and Lohanick (1985) and Asmus and Grant (1999).

Due to the fixed location of the ship and various snow events (heavy snowfalls, wind redistribution, etc.), thin snow was located near the ship in the incidence angle range 30–40° in the radiometers field of view (footprint of 4×4 m at 30°), as the thicker snowpacks were in the range 50–70° (footprint of 30×30 m at 70°). Only morning measurements were employed in this study to avoid diurnal influence on the brightness temperatures, as higher correlation between brightness temperatures and SWE is found in dry and cold snow (Drobot & Barber, 1998). Furthermore, previous studies showed that small amounts of liquid water contribute significantly to microwave emission (e.g., Foster et al., 1999; Harouche & Barber, 2001), which in turn decreases SWE prediction accuracy.

3. Results and discussion

3.1. Snow properties

3.1.1. Thin snow temporal evolution

Total SWE values decreased toward the end of the sampling period, as averaged SWE between the beginning of the sampling period and day 3 was 18.8 mm and 11.8 mm between days 83 and the end of the sampling period (Fig. 3a). Here we focus on a presentation of the brine, temperature and phase proportions of the snow as these directly affect the dielectric properties of the snow. The lowest averaged values of snow wetness occurred at the top of snowpack during the cooling and the warming (0.6% and 1.2%) periods, respectively (Fig. 3b). Average wetness values at the bottom of the snow pack were 4.5% and 4.3% for both time periods. A significant increase was observed during the warming period (starting on day 58) where values oscillated between 4% and 6% between day 100 and day 108 (Fig. 3b). Snow grain size remained stable until day 58, after which an increase occurred until day 83 where maximum values were reached (Fig. 3c).

Both air and snow/ice interface temperatures decreased between the beginning of the sampling period and day 58 where they reached a minimum of −37.6 and −31.8 °C for T_{air} and T_{si}, respectively (Fig. 2). The warming period was characterized by a significant increase in both T_{air} and T_{si} where values reached −4.1 and −7.0 °C around day 125, respectively.

Modeled snow electrical properties showed that during the cooling period high permittivity values are found in the middle of the snow layer (Fig. 4a). The highest values were measured around day 31 (near 1.8 for 19 GHz) and the lowest values modeled around day 15 (below 1.4 at all frequencies). During the warming period, maximum modeled values occurred in the top layer between day 100 and 103 where the permittivity reached 1.88, 1.81 and 1.79 for 19, 37 and 85 GHz, respectively (Fig. 4a). No significant trends in dielectric loss were measured

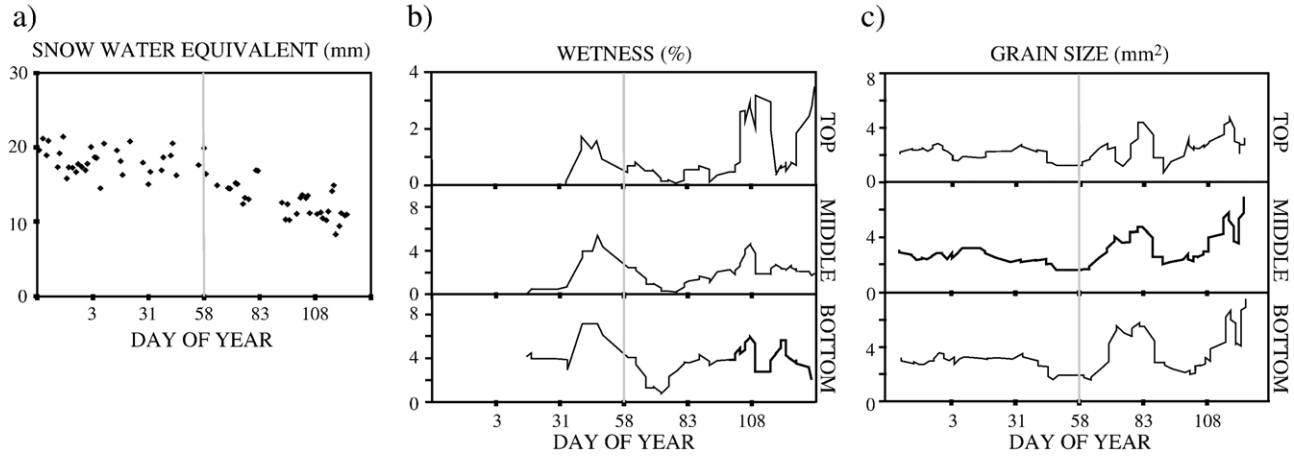

Fig. 3. Total snow water equivalent values (a), water in liquid phase (b) and snow grain size (c) for thin snow covers.

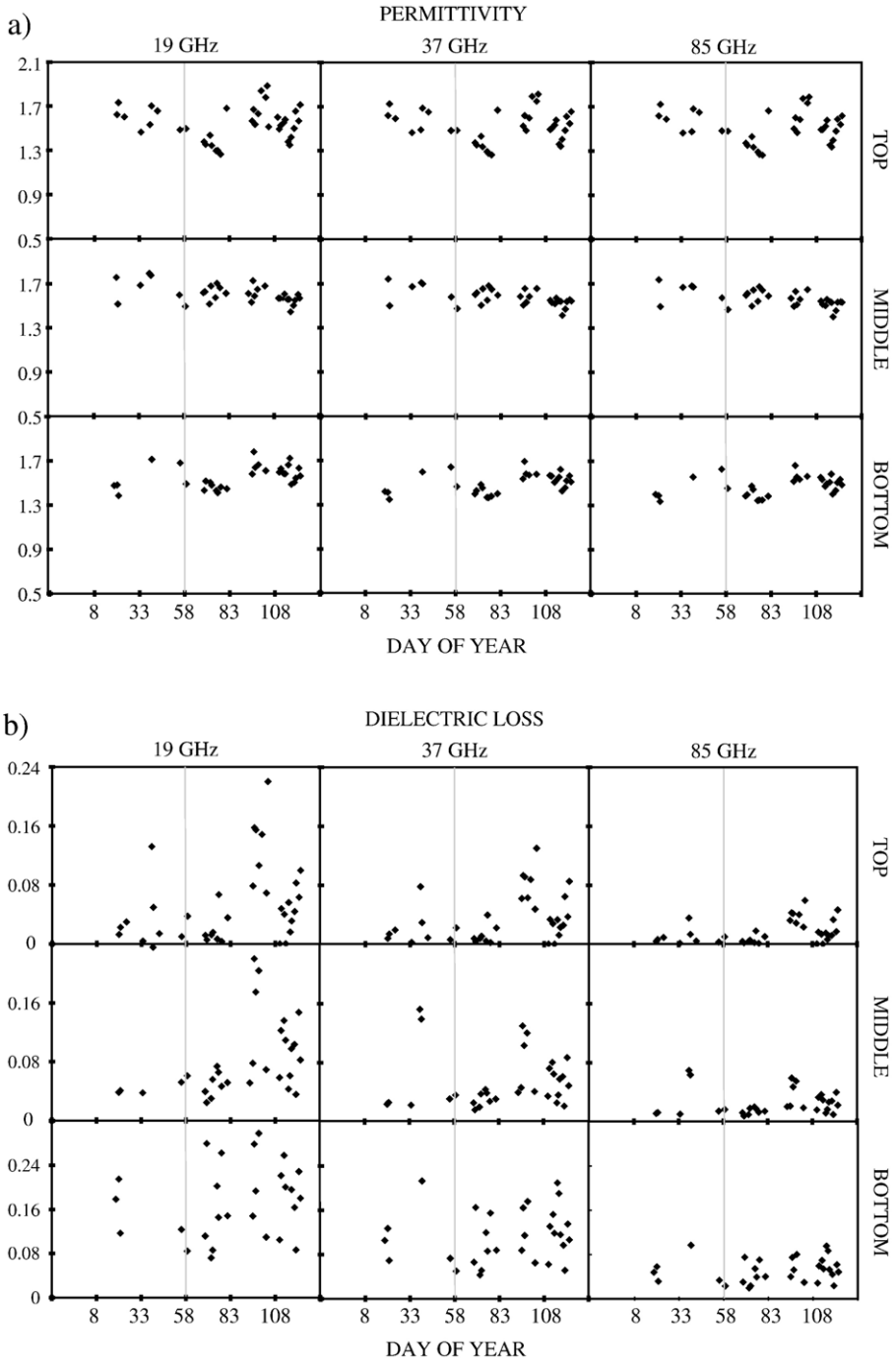

Fig. 4. Temporal evolution of snow permittivity (a) and dielectric loss (b) for 19, 37 and 85 GHz for thin snow covers.

for the cooling period (Fig. 4b). The warming period was characterized by an increase in the middle and top layers for 19, 37 and 85 GHz, respectively. A significant increase was measured on day 103 for 19 and 37 GHz where values tripled from an average of 0.04 to 0.12 (Fig. 4b).

The observed decrease in permittivity between day 35 and 83 was attributable to a coincident decreasing trend in wetness (Fig. 3b). Permittivity of the snowpack depends upon this physical property; increased wetness values would decrease the ability of the medium to permit the incident microwave radiation (e.g., Barber et al., 1995; Comiso et al., 1989; Hallikainen, 1989; Lohanick, 1993; Pulliainen & Hallikainen, 2001; Ulaby et al., 1986). Concordant to the decrease in snow density and temperature, wetness values also decreased from values varying around 2% (day 40) to 0% (day 70) at the top layer and from 7% to 2% at the bottom layer for the same period (Fig. 3b). A substantial increase in complex permittivity between day 83 and day 108 was attributable to increasing snow wetness.

3.1.2. Thick snow temporal evolution

The temporal pattern of SWE (Fig. 5a) followed the snow thickness evolution. Increases were recorded on days 5 (from 18

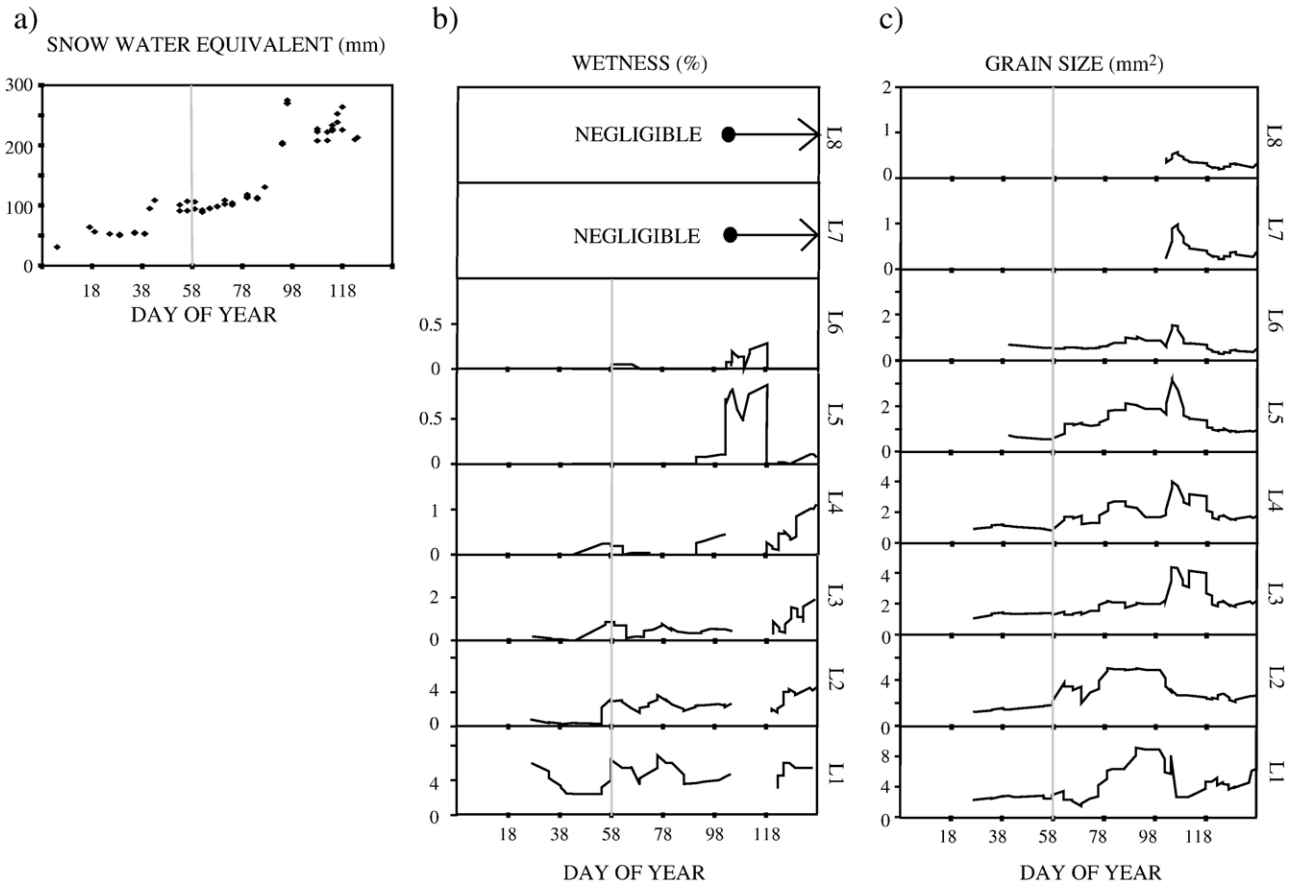

Fig. 5. Total snow water equivalent values (a), water in liquid phase (b) and snow grain size (c) for thick snow covers.

to 30 mm), 42 (from 50 to 100 mm) and 91 (from 110 to 200 mm) when significant snowfall occurred (Fig. 5a). High liquid water values were measured at the bottom of the snowpacks (layers L1 and L2) with values oscillating between 3% and 8% throughout the period (Fig. 5b). Missing values between day 91 and day 110 were attributable to the flooding of the basal layers (layers L1 to L4) as the local buoyancy was exceeded due to the weight of the overlying thick snowpack. Snow grain size values increased significantly between day 60 and 90 from L1 to L5 (Fig. 5c). A significant peak was measured around day 100 for L3 to L7 concordantly to the flooding of the basal layer. Please refer to Langlois et al. (in press) for the details on the impact of the flooding on snow properties.

As described in Section 3.1.1 (thin snow covers), the minimum air temperature was measured on day 57 at −37.6 °C (Fig. 6); however, the minimum at the snow/ice interface was measured on day 62 (−25.4 °C). The increase in T_{si} during the warming period was stable with a maximum value of −5.2 °C on day 124 coincidently with the substantial increase in T_{air} between days 118 and 124.

During the cooling period (Fig. 7a), the highest permittivity values were modeled at L3 (varying around 1.7) and the lowest values at L5 (varying around 1.4) for all three frequencies. Values at L8 increased towards the end of the sampling period as they decreased at L5. Three individual samples were displayed after day 110 for L1 and their permittivity values were the highest (between 1.7 and 1.9). Dielectric loss was higher towards the bottom of the snowpack throughout the cooling period (Fig. 7b). However, the warming period showed a significant increase around day 95 at L5, where values jumped from nearly 0 to about 0.09, 0.07 and 0.05 for 19, 37 and 85 GHz, respectively.

Layer L8 had lower permittivity values with a negligible dielectric loss due to the occurrence of a dry and fresh snow layer for the most of period (Fig. 7a and b). The significant

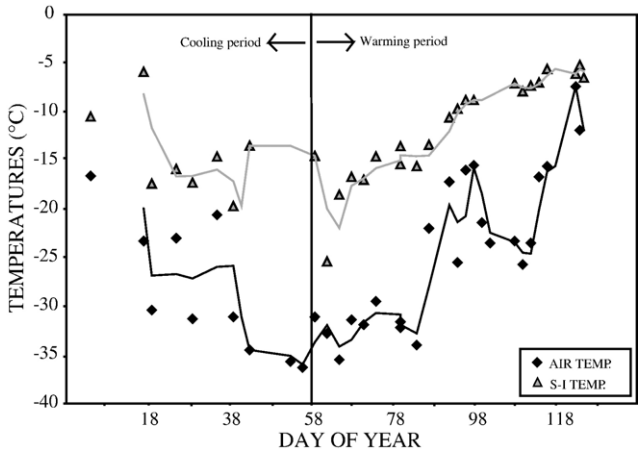

Fig. 6. Air and snow/sea ice (S-I) interface temperatures temporal evolution for thick snow covers (the lines represent a 2-day moving average on the temperatures).

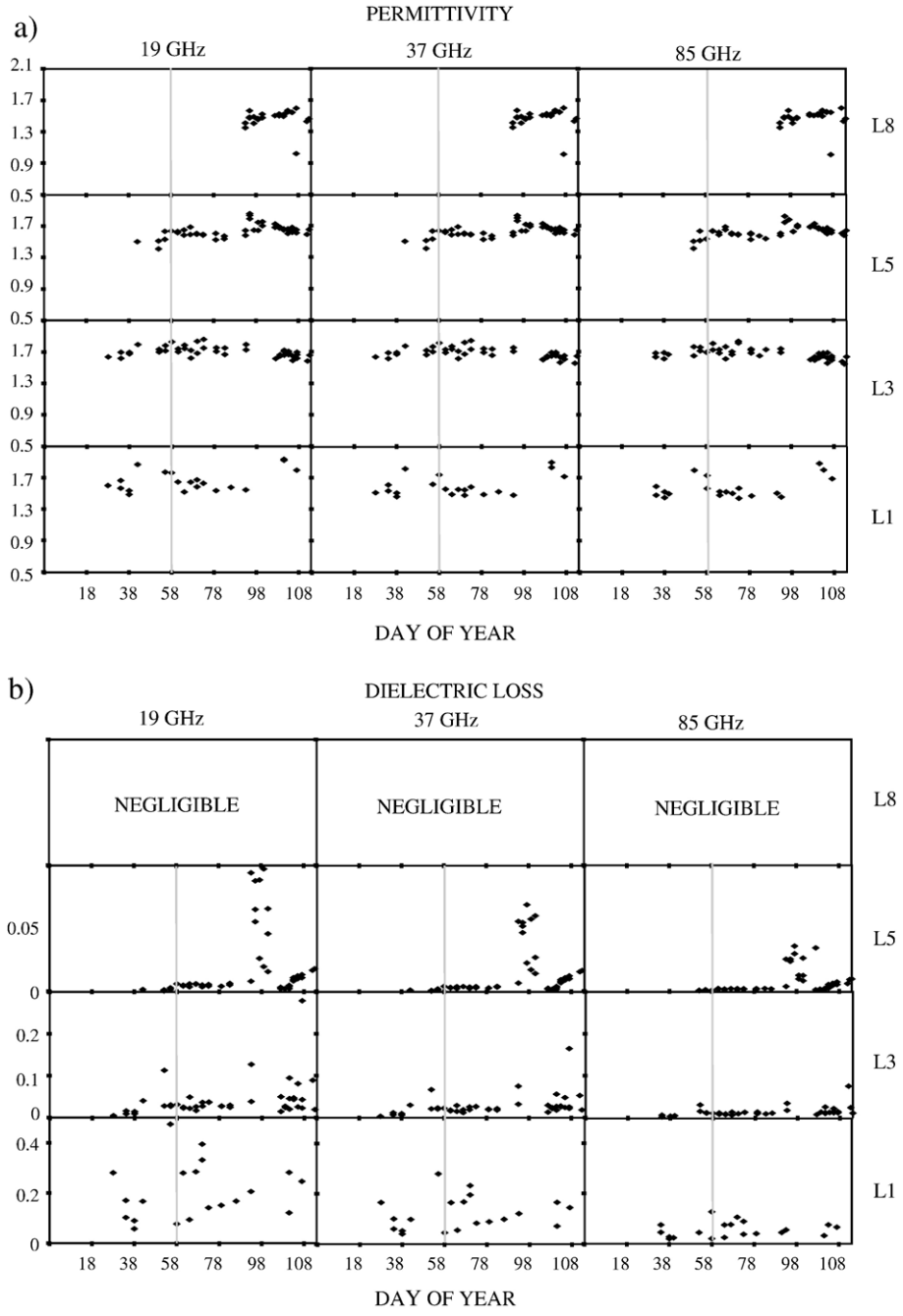

Fig. 7. Temporal evolution of modeled snow permittivity (a) and dielectric loss (b) for 19, 37 and 85 GHz for thick snow covers.

increase in permittivity in L5 after day 91 was attributed to the upward transport of the brine volume forced upward from the underlying layer by capillarity suction following the flooding period (Langlois et al., in press). We also observed an increase in permittivity in layer L1 in three different samples between days 110 and 120, concordant with very high brine volume values, again due to the flooding within this particular layer.

3.2. Passive microwave emission

For each set of coupled snow pit and passive microwave measurements, five replicate multi-angle scans were conducted along with 30 sample points at an incidence angle of 53°. The brightness temperature precision depends upon the frequency/polarization combination and range anywhere between 0.1 K and 0.5 K throughout our sampling period for both fixed and multi-angular measurements.

3.2.1. Thin snow T_b temporal evolution

Brightness temperatures decreased slightly during the cooling period (day 344–57) for all frequencies between incidence angles of 30° and 40° where values ranged between 240 K and 260 K (Fig. 8a and b). Maximum brightness temperatures during the cooling period were measured on day 357 for all

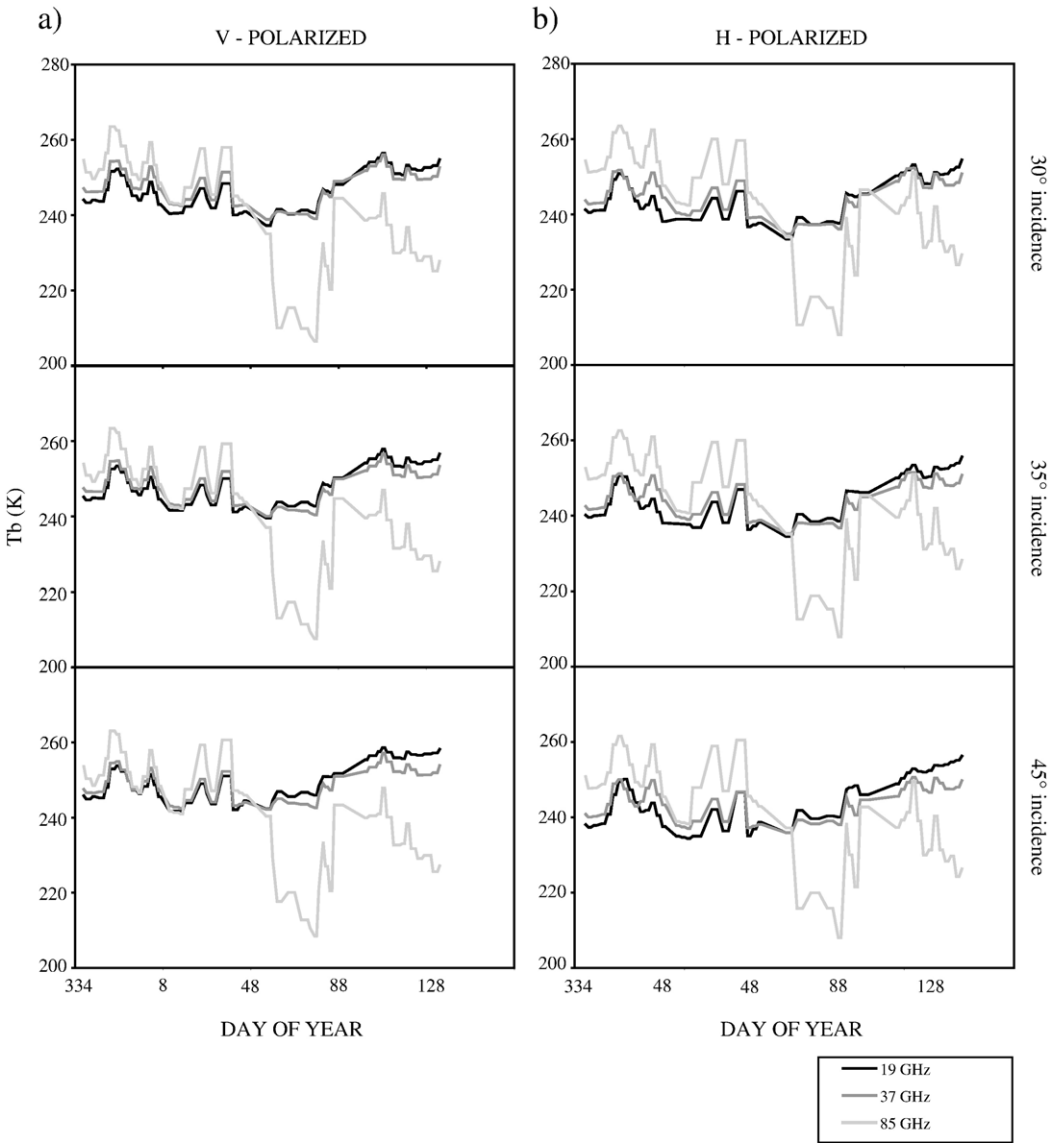

Fig. 8. Brightness temperatures (T_b) temporal evolution for 19, 37 and 85 GHz in both vertical (a) and horizontal (b) polarizations over thin snow covers between 30° and 40° of incidence angle.

three frequencies. Furthermore, variations in T_b were greater at 85 GHz with values oscillating between 265 K and 240 K throughout the cooling period.

During the warming period, a decrease in T_b was noticeable at 85 GHz (between days 58 and 83) where values decreased from an average of 250 K to approximately 215 K (Fig. 8a and b). Between day 80 and day 100, T_bs increased from 215 K to 240 K, then decreased to an average of 230 K until the end of the sampling period for both horizontal (Fig. 8a) and vertical (Fig. 8b) polarizations.

The peak in T_b on day 357 was coincident with a significant increase in T_{air} (−13.3 °C) at the time of the SBR measurements. Both air and brightness temperatures decreased thereafter until the minimum value was achieved on day 57. Variations measured during the cooling period were mainly due to variations in air temperatures since low variations were noticed in the snow physical properties.

T_bs decreased at 85 GHz after day 58, coincidently to significant increase grain size (Fig. 3c) (e.g., Foster et al., 1999; Matzler, 1987) as frequencies are more sensitive to increasing grain size within the snow (e.g., Foster et al., 1999). Maximum grain size values varied from 4 to 6 mm (Fig. 3c) depending on the vertical location and would increase volume scattering at high frequencies (e.g., Drinkwater & Crocker, 1988; Hallikainen, 1989; Kelly et al., 2003; Tiuri et al., 1984; Tsang et al., 2000). Afterwards, T_b values at all frequencies coincidently increased with increasing wetness (i.e., increasing permittivity and dielectric loss) until approximately day 108 where values were maximum (Fig. 4). The peak in permittivity is stronger at the top layer as it is quite important at top and middle layers for dielectric. The wetness increased from 0.5% to 3%, 2% to 4% and 4% to 6% for top, middle and bottom layers, respectively. The presence of liquid water within the snowpack increases the internal absorption, permittivity and dielectric loss along with

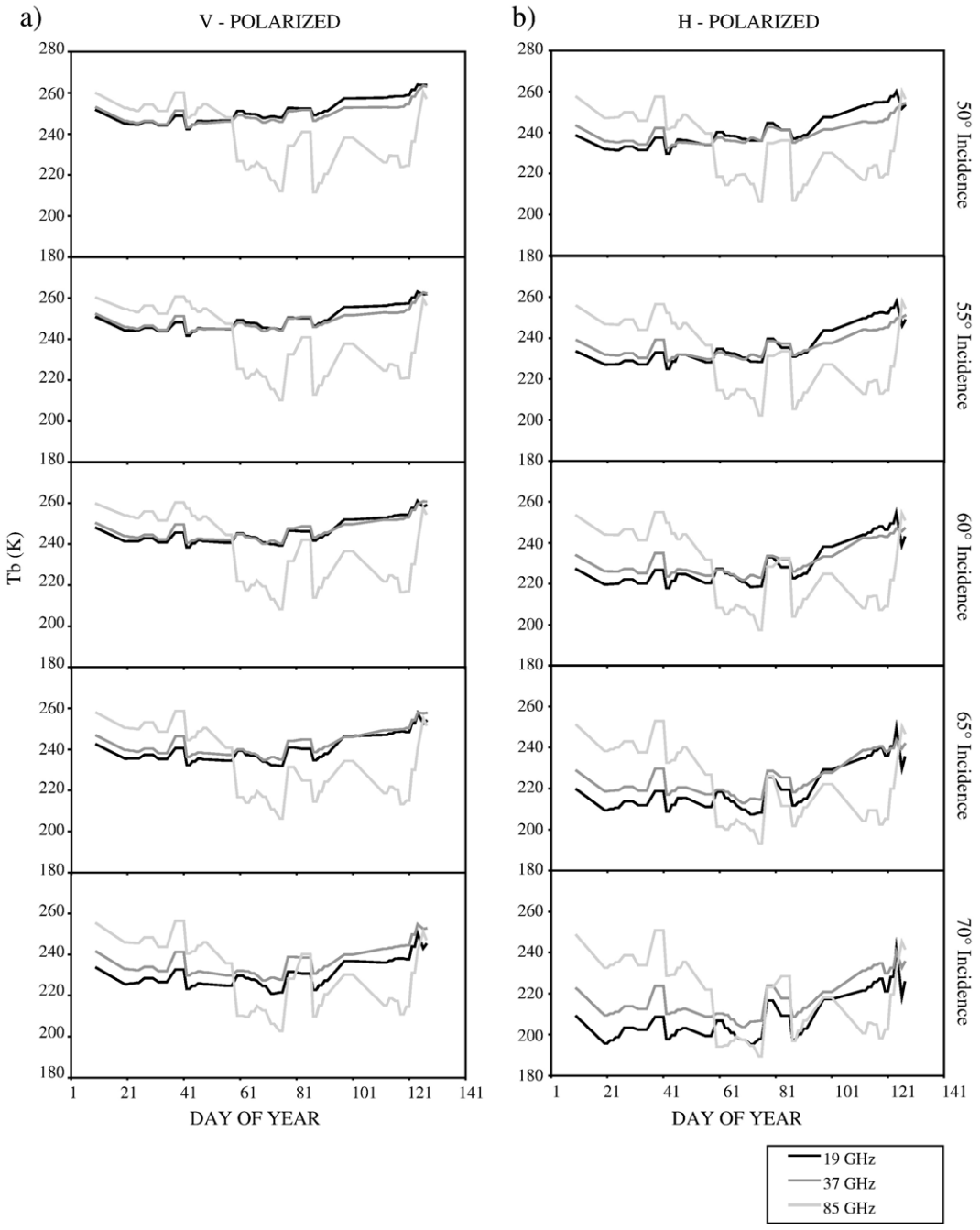

Fig. 9. Brightness temperatures (T_b) temporal evolution for 19, 37 and 85 GHz in both vertical (a) and horizontal (b) polarizations over thick snow covers between 50° and 70° of incidence angle.

decreasing volume scattering (Foster et al., 1984). Wet snow brightness temperatures will increase (towards a black body behavior where $T_bV = T_bH$) at vertical polarization as shown in Fig. 8a (e.g., Garrity, 1992; Stiles & Ulaby, 1980; Ulaby et al., 1986; Walker & Goodison, 1993).

3.2.2. Thick snow T_b temporal evolution

No significant trends in thick snow T_bs were observed during the cooling period at all frequencies and incidence angles (Fig. 9a and b). The maximum T_bs were measured at 85 GHz in the vertical polarization (values varying around 265 K at an incidence angle of 50° Fig. 9a). Minimum T_bs were recorded at 19 GHz in the horizontal polarization (values varying around 190 K at 70° in Fig. 9b).

The warming period was characterized by a slow and steady increase for the T_b of thick snowpack for both vertical and horizontal polarizations (Fig. 9a and b). A significant peak was measured between day 72 and day 84 at all frequencies and angles. The depolarization decreased significantly during this period especially for 19 GHz with an incidence angle of 70°.

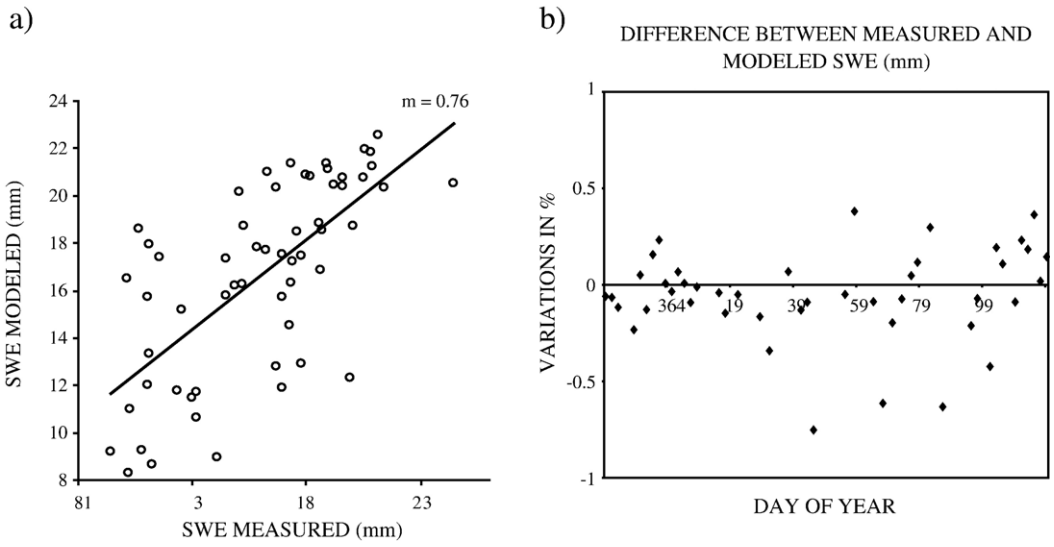

Fig. 10. Comparison between the modeled and measured SWE values (a) and the temporal evolution of the variation (b) for thin snow covers.

Generally, the depolarization decreased throughout the warming period except for individual cases at 19 GHz between days 117 and 124.

The steady cooling period T_bs were linked to the negligible changes in snow thermophysical properties until day 57. Little variations during this cooling period were coincident with the increase in T_{air} as reported in numerous studies (e.g., Grody & Basist, 1996; Lohanick, 1993; Rosenfeld & Grody, 2000; Sokol et al., 1999). Air temperature significantly increased from −23 to −14 °C, −28 to −21 °C and from −30 to −19 °C for days 357, 6 and 28, respectively. T_b values at 85 GHz were higher than 19 and 37 GHz throughout the cooling period. However, it was not possible to relate this behavior with the snow cover properties as the physical/electrical properties data set only starts on day 6. A possible cause for the T_bs at 85 GHz to be so high could be the relatively warm snow/ice interface temperature (T_{si}) measured under thicker snowpacks. Increasing air temperature increases the liquid water volume in the snow cover decreasing the difference between vertical and horizontal polarization (ΔP) as wet snow has a theoretical ΔP of 0 (Garrity, 1992; Matzler & Huppi, 1989).

During the warming period, T_b values increased significantly until the end of the sampling period concordant to warming air temperature. There are no significant correlations between the dielectric properties and the variations observed in T_bs. However, the maximum in permittivity and dielectric loss around day 103 is concordant to an increase in wetness from the flooding of the basal layers (Fig. 7). The increase did occur at all layers; however, no data are available from L1 to L4 as it was practically impossible to sample (Langlois et al., in press). Variations were greater at horizontal polarization and wide incidence angle, as observed in the cooling period and numerous studies over land and first-year sea ice (e.g., Barber & LeDrew, 1994; Derksen et al., 2000, 2005; Hallikainen, 1989).

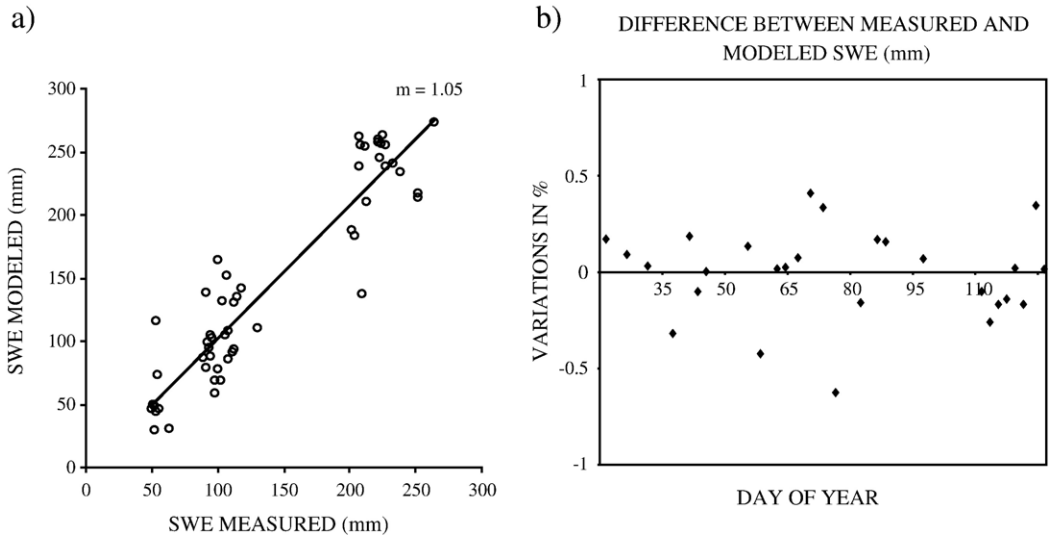

Fig. 11. Comparison between the modeled and measured SWE values (a) and the temporal evolution of the variation (b) for thick snow covers.

The increase between day 72 and day 84 was coincident with a significant increase in air temperature. Another increase was measured on day 91; however, this increase is a consequence of flooding that occurred within the basal layers. Such an intrusion of liquid water significantly increases the microwave emission as mentioned in Section 3.2.1 (e.g., Hallikainen et al., 1986; Thomas & Barber, 1998; Tiuri et al., 1984) at L1 (Fig. 7a and b).

3.3. Algorithm development

A common approach for developing new SWE statistical algorithms is to use a multiple regression with two independent variables (SWE and T_{air}) and one dependent variable (brightness temperatures). We evaluate the normality of T_{air}, SWE and the associated brightness temperatures using a Lilliefors test for goodness of fit.

3.3.1. Thin snow covers

From the normality score results, a candidate algorithm is proposed at horizontally polarized 19 GHz with an incidence angle of 40° (19H40). Using multiple regression analysis on the dependent variable (T_b) and independent variables (T_{air} and SWE), we proposed the following algorithm:

$$SWE_{THIN} = \frac{(T_b19H_{40°} - 277.01 - 0.57T_{air})}{-1.15} \quad (5)$$

The comparison between modeled and measured SWE showed a good correlation with a R^2 of 0.7 and a slope of 0.76 (Fig. 10a). Lower incidence angle did not show better results with R^2 values of 0.55 and 0.66 for 30° and 35°, respectively. The temporal evolution of the residuals showed less scatter during the cold period than the warm period (lower dielectric constant in the cold period), which was divided on day 57 (Fig. 10b). The measured variations in % can be explained by the spatial variability of snow thickness in the thin snow sampling area (Langlois et al., in press). Furthermore, the radiometer's ground field of view was approximately 5 × 5 m from a height of 12 m. This area is much larger than a snowpit, which is approximately 0.4 × 0.4 m. For example, over a thin snow cover, a difference between 4 cm and 6 cm in snow thickness can create difference up to 5–10 mm in SWE (up to 50%) depending on the density of the missing thickness. As the sampling was arranged so that thin snow covers were sampled only, little variations in spatial thickness distribution will cause errors in SWE predictions.

3.3.2. Thick snow covers

From the normality test in the thick snow covers, 19H55 is used in order to retrieve thick snowpacks SWE values. We use multiple regression with SWE and air temperature to propose the following algorithm to estimate SWE for thick snow covers:

$$SWE_{THICK} = \frac{(T_b19H_{55°} - 235.33 - 0.43T_{air})}{0.1} \quad (6)$$

Using the above algorithm, very good agreement between the measured and modeled SWE was obtained ($R^2 = 0.94$ in Fig. 11a). The incidence angle is within 2° of what is used from spaceborne satellite passive microwave remote sensing (53° for SSM/I and 54° for AMSR-E). Our data set at 53° was not as complete as 55° (from the multi-angle analysis), and the transition between thin and thick snow was too close, at 40° and 50°. Therefore, we choose the data at 55° to ensure the stability of the snow thickness. However, we can assume that the algorithm at 55° would be applicable for incidence angles of 53–54°. The slope of 1.05 indicated very little bias from our proposed algorithm. The temporal evolution of the residuals between the measured and the modeled SWE showed the stronger variations in the warming period between day 58 and 127 (Fig. 11b), which were concordant with increasing temperatures as the liquid water from melting affects the T_b signatures significantly (e.g., Barber et al., 2003; Lohanick & Grenfell, 1986; Markus & Cavalieri, 1998; Pulliainen & Hallikainen, 2001; Singh & Gan, 2000; Walker & Goodison, 1993). The minimum differences between measured and modeled SWE were found during the coldest period of the sampling period between day 57 and day 67.

In both thin and thick snow covers, 19 GHz in the horizontal polarization showed better correlation with SWE when compared to 37 GHz. We used the same approach using the normalized brightness temperatures between 19 and 37 GHz (T_b19–T_b37), but the results on the SWE prediction were not as good in both cases. This difference is normally used for SWE retrieval over land, but the concept over sea ice more complicated due to brine volume vertical migration in the snowpack, which affects the permittivity and dielectric loss differently at both frequencies. The multiple regression results were significant when using 37 GHz but the best results were obtained using 19 GHz. Over such a wide range of snow thickness, it is not surprising to see good agreement between measured and modeled SWE values since lower frequencies absorption is lower especially in thick snow covers. Furthermore, with the very high density values in thin snow covers (i.e., high permittivity), lower frequencies will interact enough with the snow cover so that an algorithm can be developed from such frequencies. Both the thin and thick snow cases use all of the available morning data in the regression, which this means that the comparison will be stronger than expected with an independent comparison. Therefore, these comparisons are 'optimal' as they are done on a dependent data set.

4. Conclusions

During the cooling period, the snowpack was characterized by very little changes in thermophysical properties. The results showed that the variations in T_bs for thin snow over the cooling period were mainly attributable to changes in air temperature with fairly constant snow physical properties. The warming period was characterized by significant changes in high frequency T_bs, coincidently with increasing grain size (i.e., increasing volume scattering), temperatures and liquid water content (increasing absorption).

The thick snowpack properties also show little variation during the cooling period and brightness temperatures were

again strongly linked to air temperature. Significant changes occurred during the warming period with flooding of the snow basal layers that significantly increased microwave emission. Therefore, T_bs were strongly linked to water content (towards a black body behavior), which furthers our understanding of our SWE prediction variations.

The algorithm over thin snow covers used 19H40 as the best frequency/polarization/incidence angle combination for multiple regression with T_{air} and SWE. Throughout the observational period, good correlation was found for this algorithm when compared with field data. The algorithm performed better during the cold and dry period due to very limited metamorphism during this period. The differences were attributed to the variations in T_{air} and snow wetness, which affects the T_b without significantly affecting the SWE values. Scale difference (spatial heterogeneity) between the radiometer (m^2) and the snow pit (cm^2) also played a role in the SWE prediction variations.

The same statistical approach was used to retrieve SWE from thicker snowpacks. Results showed that the 19H55 combination gave the best prediction results. Validation of the proposed algorithm also showed significant results between the observed and modeled data. We explain the prediction errors with sudden variations in air temperature and flooding (starting on day 91) that significantly increased the T_b. Furthermore, spatial heterogeneity in snow thickness also contributed in the SWE prediction variations (Derksen et al., 2005) since the radiometer measured thick snow cover emissivity at wide incidence angles (50–70°) when compared to thin snowpacks (30–40°).

Generally, our proposed algorithms performed quite well throughout the study period. However, our thin snow data set was limited in terms of incidence angles and it is most likely that the results would be better closer to the Brewster angle (angle where the microwave emission is maximum) and, therefore, easier to apply to a satellite remote sensing approach. The performance of both algorithms was stronger at cold temperatures, with dry snow and little changes in the thermophysical properties (Langlois et al., in press). From the algorithms perspective, the sensitivity to air temperature decreased with increasing thickness. Variation in air temperature over thin snow covers had a greater impact on the T_b variations when compared with thick snow covers. For example, with a constant measured SWE value, an sudden increase of 10 °C in T_{air} means an uncertainty of approximately 45% over thin and 17% over thick snowpacks. This is why the most important variations occurred in the transition seasons (fall–winter and winter–spring) where the air temperatures vary on a daily basis.

Current work on the exploitation of all incidence angles over a wider range of snow thickness will be conducted. Results should improve our understanding and capacity of predicting seasonal SWE over first-year sea ice with respect to snow thickness, especially over thin snow covers. We proposed thin and thick SWE algorithms; however, we are not sure what thickness should be the marker between thin and thick SWE algorithms. Our next field season will investigate this matter in order to know when to apply either a thin or thick SWE algorithm. Future work on the empirical relationships between in situ active microwave measurements (C-Band 5.3 GHz scatterometer) and SWE will be explored in order to develop a snow depth algorithm that will ultimately be coupled with our passive microwave results presented in this paper. Ultimately, this in situ work coupling passive and active microwave data with SWE will be scaled up to passive and active microwave satellite remote sensing. So far, microwave remote sensing has proven to be an excellent tool in the development/validation of geophysical and thermodynamic models, but further knowledge of its interactions with the surface is essential in understanding and modeling the actual climate change scenario.

Acknowledgements

This work was financially supported by grants to DGB for the CASES NSERC network, the Canada Foundation for Innovation (CFI) and the Polar Continental Shelf Project. We thank Christina Blouw, Teresa Fisico, Owen Owens, John Iacozza from the University of Manitoba and Mark Christopher Fuller and Kris Konig for tremendous assistance in the field sampling. Many thanks also to Tim Papakyriakou from the University of Manitoba and John Yackel from the University of Calgary for guidance and support throughout the experiment. Special thanks to Dr Chris Derksen from the Climate Research Division at Environment Canada for providing comments that helped to improve this manuscript. The authors also thank the crew of the CCGS *Amundsen* for an essential logistical support throughout the study.

References

Armstrong, R. L., Chang, A., Rango, A., & Josberger, E. (1993). Snow depths and grain size relationships with relevance for passive microwave studies. *Annals of Glaciology*, *17*, 171−176.

Arons, E. M., & Colbeck, S. C. (1995). Geometry of heat and mass transfer in dry snow: A review of theory and experiment. *Reviews of Geophysics*, *33*, 463−493.

Asmus, K., & Grant, C. (1999). Surface based radiometer (SBR) data acquisition system. *International Journal of Remote Sensing*, *20*, 3125−3129.

Barber, D. G., Fung, A. K., Grenfell, T. C., Nghiem, S. V., Onstott, R. G., Lytle, V. I., et al. (1998). The role of snow on microwave emission and scattering over first-year sea ice. *IEEE Transactions on Geoscience and Remote Sensing*, *36*, 13.

Barber, D. G., Iacozza, J., & Walker, A. (2003). Estimation of snow water equivalent using microwave radiometry over Arctic first-year sea ice. *Hydrological Processes*, *17*, 3503−3517.

Barber, D. G., & LeDrew, E. (1994). On the links between microwave and solar wavelengths interactions with snow covered first year sea ice. *Arctic*, *47*, 298−309.

Barber, D. G., Papakyriakou, T. N., LeDrew, E. F., & Shokr, M. E. (1995). An examination of the relation between the spring period evolution of the scattering coefficient and radiative fluxes over landfast sea-ice. *International Journal of Remote Sensing*, *16*, 3343−3363.

Barber, D. G., & Thomas, A. (1998). The influence of cloud cover on the radiation budget, physical properties and microwave scattering coefficient of first-year and multi-year sea ice. *IEEE Transactions on Geoscience and Remote Sensing*, *36*, 13.

Boer, G. J., Flato, G., & Ramsden, D. (2000). A transient climate change simulation with greenhouse gas and aerosol forcing: Projected climate to the twenty-first century. *Climate Dynamics*, *16*, 427−450.

Cavalieri, D., & Comiso, J. (2000). *Algorithm Theoretical Basis Document for the AMSR-E Sea Ice Algorithm, Revised December 1*. Landover, MD, USA: Goddard Space Flight Center.

Chang, A. T. C., Foster, J. L., Hall, D. K., Rango, A., & Hartline, B. K. (1982). Snow water equivalent estimation by microwave radiometry. *Cold Regions Science and Technology*, *5*, 259−267.

Comiso, J. C., Grenfell, T. C., Bell, D. L., Lange, M. A., & Ackley, S. F. (1989). Passive microwave in-situ observations of winter Wedell sea ice. *Journal of Geophysical Research, [Oceans]*, *95*, 10891−10905.

Derksen, C., LeDrew, E., & Goodison, B. (2000). Temporal and spatial variability of North American prairie snow cover (1988–1995) inferred from passive microwave-derived snow water equivalent imagery. *Water Resources Research*, *36*, 255−266.

Derksen, C., Walker, A., & Goodison, B. (2005). Evaluation of passive microwave snow water equivalent retrievals across the boreal forest/tundra transition of western Canada. *Remote Sensing of Environment*, *96*, 315−327.

Drinkwater, M. R., & Crocker, G. B. (1988). Modeling changes in the dielectric and scattering properties of young snow-covered sea ice at GHz frequencies. *Journal of Glaciology*, *34*, 274−282.

Drobot, S. D., & Barber, D. G. (1998). Towards development of a snow water equivalence (SWE) algorithm using microwave radiometry over snow covered first-year sea ice. *Photogrammetric Engineering and Remote Sensing*, *64*, 414−423.

Eiken, H. (2003). From the microscopic, to the macroscopic, to the regional scale: Growth, microstructure and properties of sea ice. In D. N. Thomas & G. S. Dieckmann (Eds.), *Sea ice: An introduction to its physics, chemistry, biology and geology* (pp. 22−81). Oxford, UK: Blackwell Science Ltd.

Flato, G. M., & Brown, R. D. (1996). Variability and climate sensitivity of landfast Arctic sea ice. *Journal of Geophysical Research*, *101*, 25,767−25,777.

Foster, J. L., Hall, D. K., Chang, A. T. C., & Rango, A. (1984). An overview of passive microwave snow research and results. *Reviews in Geophysics*, *22*, 195−208.

Foster, J. L., Hall, D. K., Chang, A. T. C., Rango, A., Wergin, W., & Erbe, E. (1999). Effects of snow crystal shape on the scattering of passive microwave radiation. *IEEE Transactions on Remote Sensing*, *37*, 1165−1168.

Francis, J. A., Hunter, E., Key, J. R., & Wang, X. (2005). Clues to variability in Arctic minimum sea ice extent.*Geophysical Research Letters*, *32*, L21501, doi:10.1029/2005GL024376 (4 pages).

Garrity, C. (1992). Characterization of snow on floating ice and case studies of brightness temperature changes during the onset of melt. In F. Carsey (Ed.), *Microwave remote sensing of sea ice* (pp. 313−328). Washington: American Geophysical Union.

Golden, K. M., Ackley, S. F., & Lytle, V. I. (1998). The percolation phase transition in sea ice. *Science*, *282*, 2238−2241.

Grenfell, T. C., & Lohanick, A. W. (1985). Temporal variations of the microwave signatures of sea ice during late spring and early summer near Mould Bay NWT. *Journal of Geophysical Research*, *90*, 5063−5074.

Grody, N., & Basist, A. (1996). Global identification of snow cover using SSMI measurements. *IEEE Transactions on Geoscience and Remote Sensing*, *34*, 12.

Hallikainen, M. T. (1989). Microwave radiometry of snow. *Advances in Space Research*, *9*, 267−275.

Hallikainen, M., & Winebrenner, D. P. (1992). The physical basis for sea ice remote sensing. Microwave remote sensing of sea ice. *Geophysical Monograph Series*, *68*, 29−44.

Hallikainen, M. T., Ulaby, F. T., & Abdelrazik, M. (1986). Dielectric properties of snow in the 3 to 37 GHz range. *IEEE Transactions on Antennas and Propagation*, *AP-34*(11), 1329−1340.

Harouche, I., & Barber, D. G. (2001). Seasonal characterization of microwave emission from snow covered first-year sea ice. *Hydrological Processes*, *15*, 3571−3583.

Intergovernmental Panel on Climate Change (IPCC). (2001). *Climate change 2001: The Scientific Basis, Contribution of Working Group I to the Third Assessment Report of the Intergovernmental Panel on Climate Change.* New York: Cambridge University Press.

Kelly, R., Chang, A. T. C., Tsang, L., & Foster, J. (2003). A prototype AMSR-E global snow area and snow depth algorithm. *IEEE Transactions on Geoscience and Remote Sensing*, *41*, 230−242.

Kunzi, K. F., Patil, S., & Rott, H. (1982). Snow cover parameters retrieved from Nimbus-7 Scanning Multichannel Microwave Radiometer (SMMR) data. *IEEE Transactions on Geoscience and Remote Sensing*, *20*, 452−467.

Langlois, A., Mundy, C.J., & Barber, D.G. (in press). On the winter evolution of snow thermophysical properties over landfast first-year sea ice. Hydrological Processes, March.

Ledley, T. S. (1991). Snow on sea ice: Competing effects in shaping climate. *Journal of Geophysical Research*, *96*, 17,197−17,208.

Lohanick, A. W. (1993). Microwave brightness temperatures of laboratory-grown undeformed first-year ice with an evolving snow cover. *Journal of Geophysical Research, [Oceans]*, *98*, 4667−4674.

Lohanick, A. W., & Grenfell, T. C. (1986). Variations in brightness temperature over cold first-year sea ice near Tuktoyaktuk, NT. *Journal of Geophysical Research, [Oceans]*, *91*, 5133−5144.

Markus, T., & Cavalieri, D. J. (1998). Snow depth distribution over sea ice in the southern ocean from satellite passive microwave data. *Antarctic sea ice physical processes, interactions and variabilityAntarctic research series*, *vol. 74*. (pp. 19−39) Washington: American Geophysical Union.

Matzler, C. (1987). Applications of the interaction of microwaves with natural snow cover. *Remote Sensing Reviews*, *2*, 259−387.

Matzler, C., & Huppi, R. (1989). Review of signatures studies for microwave remote sensing of snow packs. *Advances in Space Research*, *9*, 253−265.

Moritz, R. E., & Perovich, D. K. (1996). Surface heat budget of the Arctic science plan. *ARCSS/OAII report number 5* (pp. 64). Seattle: University of Washington.

Mundy, C. J., Barber, D., & Michel, C. (2005). Variability of snow and ice thermal, physical and optical properties pertinent to sea ice algae biomass during spring. *Journal of Marine Systems*, *58*, 107−120.

Powell, D. C., Markus, T., & Stossel, A. (2005). Effects of snow depth forcing on Southern Ocean sea ice simulations. *Journal of Geophysical Research*, *110*, 10, doi:10.1029/2003JC002212.

Pulliainen, J., & Hallikainen, M. (2001). Retrieval of regional snow water equivalent from space-borne passive microwave observations. *Remote Sensing of Environment*, *75*, 76−85.

Rosenfeld, S., & Grody, N. (2000). Anomalous microwave spectra of snow cover observed from Special Sensor Microwave Imager measurements. *Journal of Geophysical Research*, *105*, 14,913−14,925.

Rothrock, D. A., & Zhang, J. (2005). Arctic Ocean sea ice volume: What explains its recent depletion? *Journal of Geophysical Research*, *110*, 10, doi:10.1029/2004JC002282.

Singh, P. R., & Gan, T. Y. (2000). Retrieval of snow water equivalent using passive microwave brightness temperature data. *Remote Sensing of Environment*, *74*, 275−286.

Sokol, J., Pultz, T. J., & Walker, A. E. (1999). Passive and active airborne microwave remote sensing of snow cover. *Fourth international airborne remote sensing conference and exhibition/21st Canadian symposium on remote sensing, Ottawa, Canada* (pp. 8).

Stiles, W. H., & Ulaby, F. T. (1980). The active and passive microwave response to snow parameters: Part I. Wetness. *Journal of Geophysical Research*, *83*, 1037−1044.

Sturm, M., Holmgren, J., & Perovich, D. K. (2002). Winter snow cover on the sea ice of the Arctic Ocean at the surface heat budget of the Arctic Ocean (SHEBA): Temporal evolution and spatial variability. *Journal of Geophysical Research*, *107*, 16.

Tait, A. B. (1998). Estimation of snow water equivalent using passive microwave radiation data. *Remote Sensing of Environment*, *64*, 286−291.

Thomas, A., & Barber, D. G. (1998). On the use of multi-year ice ERS-1 scattering coefficient as a proxy indicator of melt period sea ice albedo. *International Journal of Remote Sensing*, *19*, 2807−2821.

Tiuri, M. E., Sihvola, A. H., Nyfors, E. G., & Hallikainen, M. T. (1984). The complex dielectric constant of snow at microwave frequencies. *IEEE Journal of Oceanic Engineering*, *OE-9*, 377−382.

Tsang, L., Chen, C., Chang, A. T. C., Guo, J., & Ding, K. (2000). Dense media radiative transfer theory based on quasicrystalline approximation with application to passive microwave remote sensing of snow. *Radio Science*, *35*, 731−749.

Ulaby, F.T., Moore, R.K., & Fung, A.K. (1986). Microwave remote sensing: Active and passive, 3, 1065–2162.

Walker, A., & Goodison, B. (1993). Discrimination of a wet snow cover using passive microwave satellite data. *Annals of Glaciology*, *17*, 6.

Walker, A., & Silis, A. (2002). Snow-cover variations over the Mackenzie River Basin, Canada, derived from SSM/I passive microwave satellite data. *Annals of Glaciology*, *34*, 8−14.

Warren, S. G., Radionov, V. F., Bryazgin, N. N., Aleksandrov, Y. I., & Colony, R. (1999). Snow depth on Arctic sea ice. *Journal of Climate*, *12*, 1814−1829.

Welch, H. E., & Bergmann, M. A. (1989). Seasonal development of ice algae and its prediction from environmental factors near Resolute, N.W.T., Canada. *Journal of Fisheries and Aquatic Sciences*, *46*, 1793−1804.

Zhou, X., & Li, S. (2002). Phase functions of large snow melt clusters calculated using the geometrical optics method. *Proc. IEEE 2002 international geoscience and remote sensing symposium (IGARSS'02). VI* (pp. 3576−3578).